SEMARAK ILMU PUBLISHING

Journal of Advanced Research in Fluid Mechanics and Thermal Sciences

Journal homepage:
https://semarakilmu.com.my/journals/index.php/fluid_mechanics_thermal_sciences/index
ISSN: 2289-7879

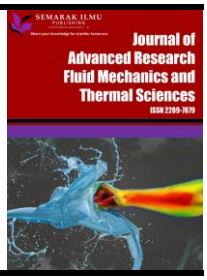

Evaluation of Elevated Temperature Oxidation of Higher Manganese Ni-Resist Alloy

Khairul Ihsan Yaakob[1], Mohd Rashidi Maarof[1,2,*], Muhammad Aminuddin Rosnizan[1]

[1] Manufacturing Research Focus Group (MFG), Faculty of Mechanical and Automotive Engineering Technology, Universiti Malaysia Pahang (UMP), 26600 Pekan, Pahang, Malaysia
[2] Automotive Engineering Centre, Universiti Malaysia Pahang (UMP), 26600 Pekan, Pahang, Malaysia

ARTICLE INFO

Article history:
Received 27 June 2024
Received in revised form 19 September 2024
Accepted 28 September 2024
Available online 20 October 2024

Keywords:
Metal casting; oxidation; Ni-Resist; nodularisation; inoculation; segregation

ABSTRACT

Nowadays Nickel was used mostly in battery, elevated temperature application and also corrosive environment. The boost of electric and hybrid vehicle had maximized the usage of Nickel as main composition in alloying industry. As such the Nickel price was at peak and become volatile to interest manufacturer. Among affected compound is Ni-Resist alloy. In this study, an alloy known as ductile Ni-resist alloy was modified to minimize its processing cost by decreasing its Nickel weight percentage. The modification was investigated in order to reduce nickel usage in the alloying composition so the alloying process cost can be minimized. More than 12 wt % chromium and manganese were alloyed with 10 wt % nickel during melting stage. Then, the evaluation of properties, oxidation behavior and its microstructure were examined. The results indicated more carbide was formed which later decreased tensile strength at elevated temperature. Oxidation resistance increased with addition of Mn/wt%. After oxidation at 765°C for 25 hours, there are oxide layers visible on the changed alloy.

1. Introduction

The last few decades have witnessed faster commercial vehicle development by each manufacturer to become more viable by each other's. To become competitive, vast research on new types of alloys was introduced to ensure their sustainability or to explore better alloy to ensure the component can be sustain on robust and demanding environment. Among highlighted alloys affected by the recent research is a material used for dynamic load at elevated temperature such as Ni-Resist alloy. Ductile Ni-Resist (DNR) alloy is one of the sub-catagories Ni-Resist alloy consist of nodule graphite shape in a structure of austenite. Austenite is useful for high temperature application due to almost all temperatures austenitic matrix alloy, high strength-to-weight ratio, good machinability, and relatively good mechanical properties at elevated temperatures. For contrast, cast iron and steel applications above 675°C temperature cross a crucial region that frequently leads to the likelihood

* *Corresponding author.*
E-mail address: mrashidi@ump.edu.my

https://doi.org/10.37934/arfmts.122.2.5261

of casting deformation and cracking. Volume changes was the suspected culprit, due to matrix phase changes from Body Centered Cubic BCC crystal structure (ferrite) to Face Centered Cubic FCC (austenite). DNR alloys, due to all temperatures austenitic matrix, do not have this transformation which become very useful for an elevated temperature application. This transformation is achieved by good practices of alloying during melting. During solidification of alloy, the 'nose' of T-T-T curve is moving towards the right [1]. As such, the solidification curve is possibly miss the curve and encourage the formation of austenitic structure. If the stage is succeeded, then the austenite may stable and remain until room temperature achieved. The occurrences of austenite were achieved without further heat treatment which minimizing the overall metal casting cost. This processing possibility give DNR alloy a competitive position in components of oil and gas, automotive or power plant compared to more expensive austenitic steel [2].

Nowadays, Nickel (Ni) was admitted as the main alloying element to transform cast iron to DNR alloy. Ni influenced metal composition during solidification and act as austenite stabilizer. It is required at 18 wt% minimum mass of Ni in the melting to encourage the austenite structure to be formed. However, Ni is known to be a comparatively expensive raw material and its high price imposes an economic restraint for alloying DNR alloy. In order to minimize the production cost, numerous researches were carried out to reduce the Ni/wt %. Some researchers proposed and trying the alloying for conversion at minimum down to 13 wt % [3]. However, changing the Ni composition on its own has conflicting effects. Therefore, during alloying, an effort was made to combine the potential of copper (Cu) and manganese (Mn). Although copper is capable of forming an austenite structure, there is possibility of Cu to counter the formation of nodule graphite shape during solidification as advised by Morrison [4]. Mn as another alloying candidate acts both as the austenite stabilizer and promotes carbide formation. Morrison also suggested that alloying with less than 4 wt% Mn could probably form a free carbide DNR alloy.

As a solution, Jincheng [5] proposed an inoculation technique to diminish the formation of carbide. Inoculation process potentially improve the distribution and the form of solidified graphite in alloy. To support the situation, Choi *et al.,* [6] discovered that inoculation improves the undercooling effect during alloy solidification by minimizing its range. So, in their research, inoculation is proposed as a potential solution for improving the undercooling effect during casting solidification. Jiyang [7] discovered solidification cooling curve might be influence through material structure refinement. The modification may be achieved by rearranges the graphite structure distribution instead of carbide distribution during inoculation stage. Using this technique, solidification cooling curves was compared relative to undercooling stage. As a result, an element segregation and the existence of secondary phases such as region last to solidify are minimized.

The literature on corrosion of DNR austenitic matrix alloy is generally limited because most researchers focused more on austenitic steel rather than austenitic iron. Dias and Lins [8] studied the scale morphology and composition of Fe-Mn-Al-Si alloy. It is observed that oxidation resistance occurs between 600 and 900^{o}C. After oxidation stages, second phases existed (oxides of Al, Mn and Fe) and acted to resist further oxidation to become worst. Tjong [9] studied the possibility of Cr and Ni being replaced by Mn to produce FeAlMnC. In his research, feasible mechanical properties at cryogenic temperature were observed. In the means time, Rashidi and Idris [10] modified Ni-Resist and evaluated the properties and its microstructure. However, the oxidation test was not carried out. Kim *et al.,* [11] studied the mechanical properties and oxidation resistance of heat resistant Si-Mo ductile cast iron. The results confirmed that the alloy can be enhanced through modifications of the alloy elements.

In order to create DNR alloy, this research aims to combine both Ni and Mn at a specific composition. A 10 wt% Ni/wt application was made in an effort to reduce alloying. Then, the Mn/wt%

combination is raised to a maximum of 12 wt%. Creating a modified alloy with an austenite structure and a graphite nodular shape is difficult. The purpose of the study is to use furnace atmosphere-air to monitor the effects of high manganese weight percentage alloy on the oxidation behavior of modified DNR. The research investigates the behaviour of furnace parts, exhaust lines, valve guides etc. at elevated temperature application of up to 765^{o}C. The objective is directed to the oxidation behaviour of the iron alloy related to metal casting microstructural inhomogeneity. The emphasis is deemed important due to the fact that the application of DNR alloy means that components are exposed to a moderately high-temperature.

2. Methodology

The current investigation was conducted using an induction furnace with a 100kg capacity. A frequency ranges of 1000-3000 Hz and a utilization power of 200 kW were used. Steel waste iron, pure nickel, and other materials were mixed into the charge composition during melting. The following parameters were addressed: (a) 9 Mn-10 Ni; (b) 10 Mn-10 Ni; (c) 11 Mn-10 Ni; and (d) 12 Mn-10 Ni wt%. Ferro-manganese (FeMn) and ferro-chrome (FeCr) were allegedly added to the alloy to raise the Mn and Cr content, according to Rashidi and Idris [10]. After melting, the mixture was raised to a temperature of 1500+20^{o}C. The slag catcher was used to boost the composition's cleanliness. The melt was poured into a mold at roughly 1400 + 20^{o}C. To create a green sand mould, silica sand, water, and bentonite were combined. Then, utilizing the In-mould approach, magnesium treatment and inoculation was carried out. The mould reaction chamber received additions of 0.5 wt.% inoculation and 1.1 wt.% nodularizer as shown in Figure 1. Table 1 contains a list of the chemical compositions of each element, nodularizer, inoculant, nickel, FeMn, and FeCr. The reaction chamber's dimension and in-gate placement were both set at 120mm. A 0.2 to 0.7 mm grading-size inoculant was used in order to reduce the effect of fading and increase the dissolve process. After solidification, Y-blocks based on ASTM A439 shape were sectioned and grounded. Later, the specimen was polished with 0.3 µm alumina powder to gained microstructural specimen. Several of the sample was prepared in dimension of 15.0 x 15.0 x 2.0 mm. They were mechanically ground by SiC paper to 2400 mesh and then polished with 1.0 µm diamond paste. The samples were polished to a mirror finish and then progressively cleaned using ultrasonic agitation for 10 min in ethanol and acetone. The samples were desiccated and dried before being exposed. A horizontal furnace equipped with a sintered alumina sample holder was used to perform isothermal oxidation. The samples were subjected for 25 hours in an air-filled, 765°C furnace. The samples were placed in an off-gas furnace, where the temperature rose by 70°C each minute. A microbalance with a 1 g resolution was used to record the mass balance [12]. The corrosion kinetic curve was plotted using the mean value of the three test findings. The term "weight gains" refers to the apparent surface of the specimens. To determine the phase composition, powder XRD was used to analyze the ground oxides [10]. Scales that had grown on the specimens' surface were identified using a scanning electron microscope (SEM), and their chemical makeups were investigated using X-ray energy dispersive spectroscopy (EDS). Several oxidized specimens were coated with copper to protect the scales while a cross-sectional metallographic view was being created. The EDS model Philips XL40 system was used to do the chemical analysis. Using CuK-1 radiation, phase analysis was carried out using a Siemens D5000 X-ray diffractometer (XRD).

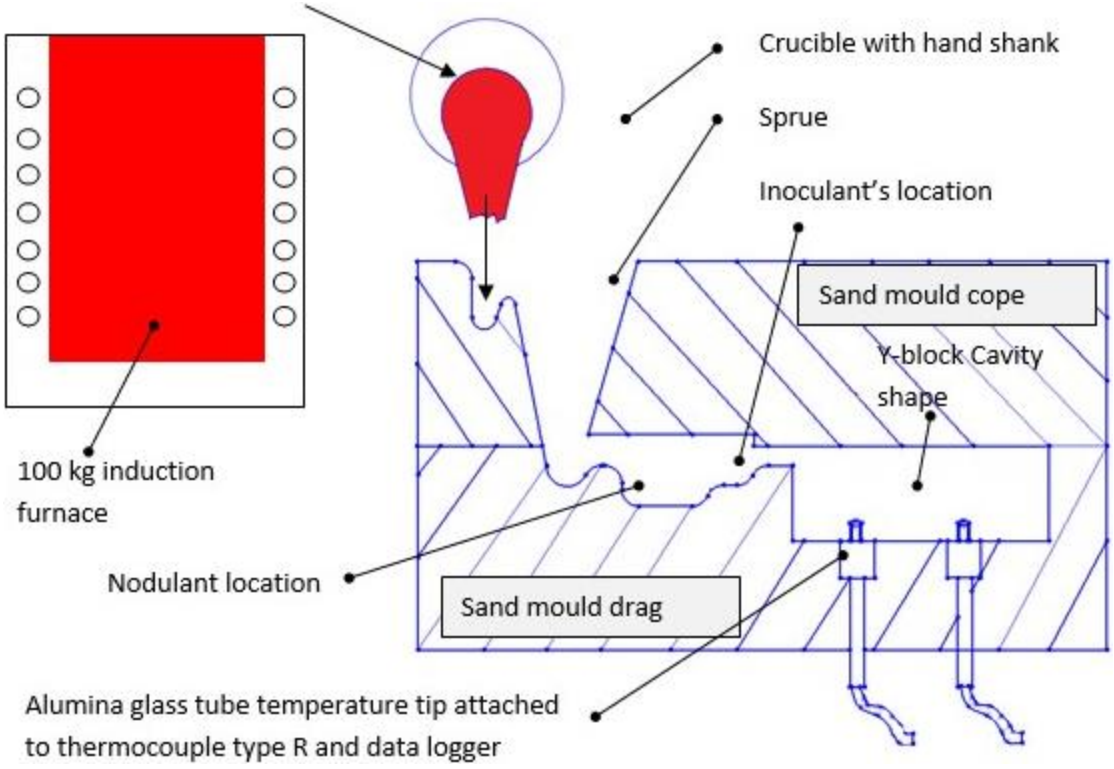

Fig. 1. Experimental setup during melting and alloying

Table 1
FeMn and FeCr (wt%), alloyed materials, nodularizer, inoculant, and chemical makeup of iron

	Element constituent										
	C	Si	Mn	P	S	Mg	Ni	Ca	Cr	R.E	Fe
MgFeSi	-	44.00	-	-	-	5.00	-	2.00	-	-	Balance
Inoculant	-	70.00	-	-	-	-	-	2.00	-	-	Balance
Pig iron	2.91	2.28	0.12	0.07	0.02	-	0.02	-	-	-	Balance
Steel	0.20	0.15	0.60	0.03	0.02	-	-	-	-	-	Balance
Nickel	-	-	-	-	-	-	99.00	-	-	-	Balance
FeMn	-	1.00	86.00	0.10	0.02	-	-	-	-	-	-
FeCr	8.00	4.00	-	0.04	0.04	-	-	-	60.0	-	-

3. Results

3.1 Microstructure Evaluation

The casting process produced a hypoeutectic composition with a number of component alloys incorporating Fe, C, Si, Mn, Ni, and other elements. Many phenomena occurred during solidification, including phase formation, element solubility, and segregation, to name a few. Further research reveals that the composition of this alloyed iron includes a variety of phases, including carbides, eutectic austenite, graphite aggregate, and austenite matrix. It is believed that Ni and Si limit the solubility of graphite in austenite while Mn increases it. Generally speaking, it is asserted that the following transformation occurs during solidification

$$L \rightarrow L_1 . L_2 \rightarrow L_1 + \gamma \quad (1)$$

An austenite iron matrix is denoted by the letters L, which stand for liquid, and the numbers L_1 and L_2, which stand for liquids rich in positive and negative segregation elements, respectively. In

contrast to the center half of the grain, which is rich in Ni and Si, the Last To Freeze (LTF) portion of the alloyed iron grain is enriched in positive segregation components like Mn as shown in Figure 2. The distribution of elements is seen in Table 2. Every alloyed iron displays the normal iron matrix when it is cast, which is made up of a mixture of austenite and carbide components, as seen in Figure 3. By using X-ray diffraction analysis, the as-cast structures were proven to contain a mixture of austenite and carbide, $Mn_{23}C_6$. The typical diffraction pattern was created by indexing the four peaks of the diffraction pattern to become the austenite's -Fe. The amount of carbide in alloyed iron varies greatly; the alloyed iron with a 12Mn-10Ni weight percentage contains the largest amounts (6.349 wt%), followed by alloys with a 6.268 wt% carbide content, a 6.037 wt% carbide content, and a 5.387 wt% carbide content. These results show that lower Ni/wt% and higher Mn/wt% ratios increased carbide formation while also stabilizing the austenite phase [1-3]. Jiyang's [7] theory implies that manganese decreases the temperature at which graphite segregates and depresses the solidification-cooling curve, which has an effect on the formation of carbide. With respect to the carbon equivalent 4.33 eutectic point, this phenomenon widens the eutectic solidifying zone. A similar occurrence increases the likelihood of carbide synthesis while reducing the possibility of free graphite. As a result, the transformation of alloyed iron in cooling austenite led to the production of a considerable amount of carbide structure.

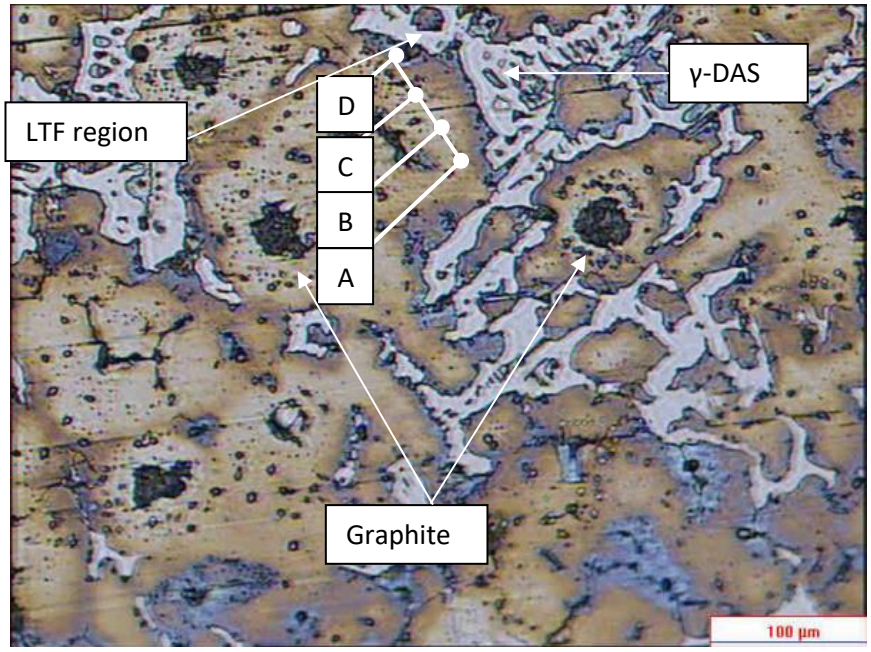

Fig. 2. The modified DNR alloy's microstructure exhibits segregation, an LTF region, austenite, and -Dendrite Arm Spacing (DAS)

Table 2
Element constituents of alloyed irons that are impacted by micro segregation (wt%)

	Electron probe position			
	Nodule graphite center (A)	Dendritic area (B)	Dendritic edge (C)	LTF Outside region, LTF (D)
FeC (graphite)	100	0	0	0
Si	0	1.192	1.174	0.738
Ni	0	7.044	5.643	4.850
Mn	0	3.924	5.426	8.556
P	0	0	0	1.437

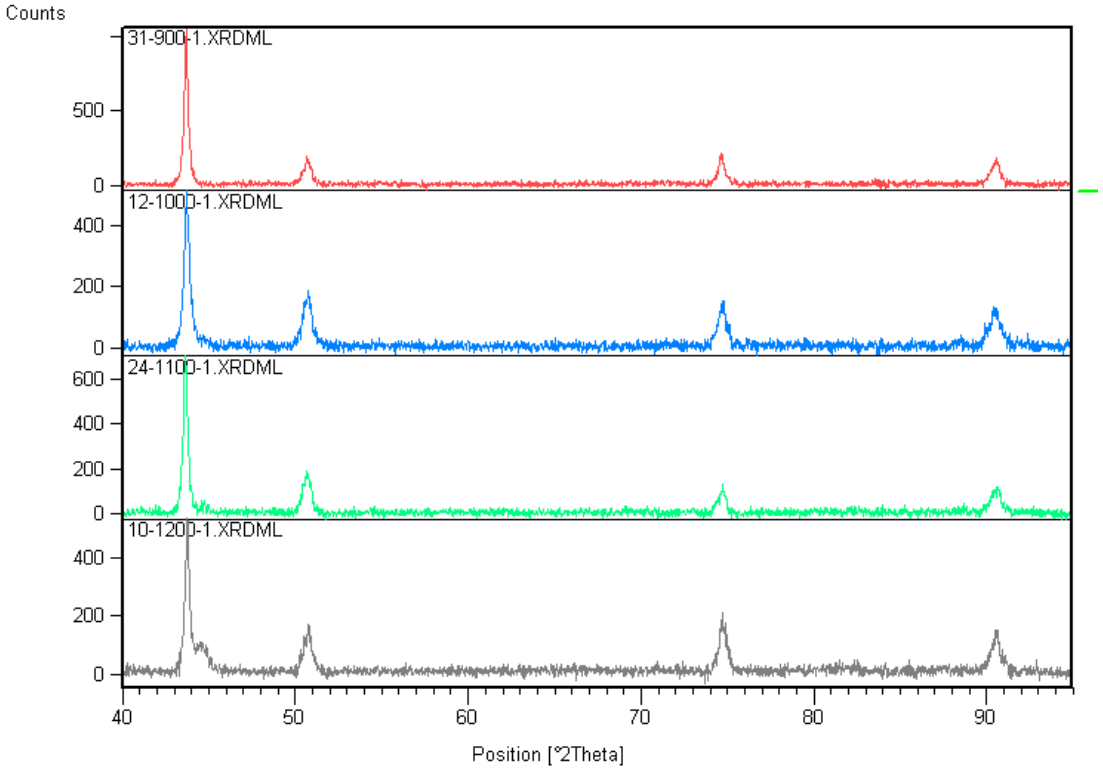

Fig. 3. Modified DNR alloy's X-ray diffraction pattern with different weight percentage

An overview of the oxide thickness and the depth of penetration following oxidation is provided in Table 3 and Figure 4. It is obvious that the Mn/wt% small reduction in oxidation depth penetration. The correlation between nodule count and alloyed iron oxide deep penetration is seen in Figure 5 and Figure 6. The alloyed iron with a 9Mn-10Ni wt% content was found to have both the maximum nodule count and oxide depth penetration. The correlation between alloyed iron oxide depth penetration and the carbide phase, $Mn_{23}C_6$, is shown in Figure 6. It was enlightening that the alloyed iron with a 9Mn-10Ni wt% content, which acquires the least carbide, has had the largest oxide depth penetration. The alloyed iron with the lowest oxide depth penetration is 12Mn-10Ni wt%, which achieves the maximum carbide composition.

Table 3
After 25 hours of exposure to furnace atmosphere-air (765°C), the specimen's average oxide thickness was measured in mm

(Mn wt. %)	Thickness (mm)	Oxide depth (mm)			Depth of attack (mm)	Depth of attack (%)
		Layer 1 (outer)	Layer 2 (inner)	Layer 3 (inner)		
12	15	0.157	0.099	0.049	0.305	2.0
11	15	0.163	0.125	0.055	0.343	2.3
10	15	0.170	0.117	0.069	0.356	2.4
9	15	0.172	0.135	0.092	0.399	2.7

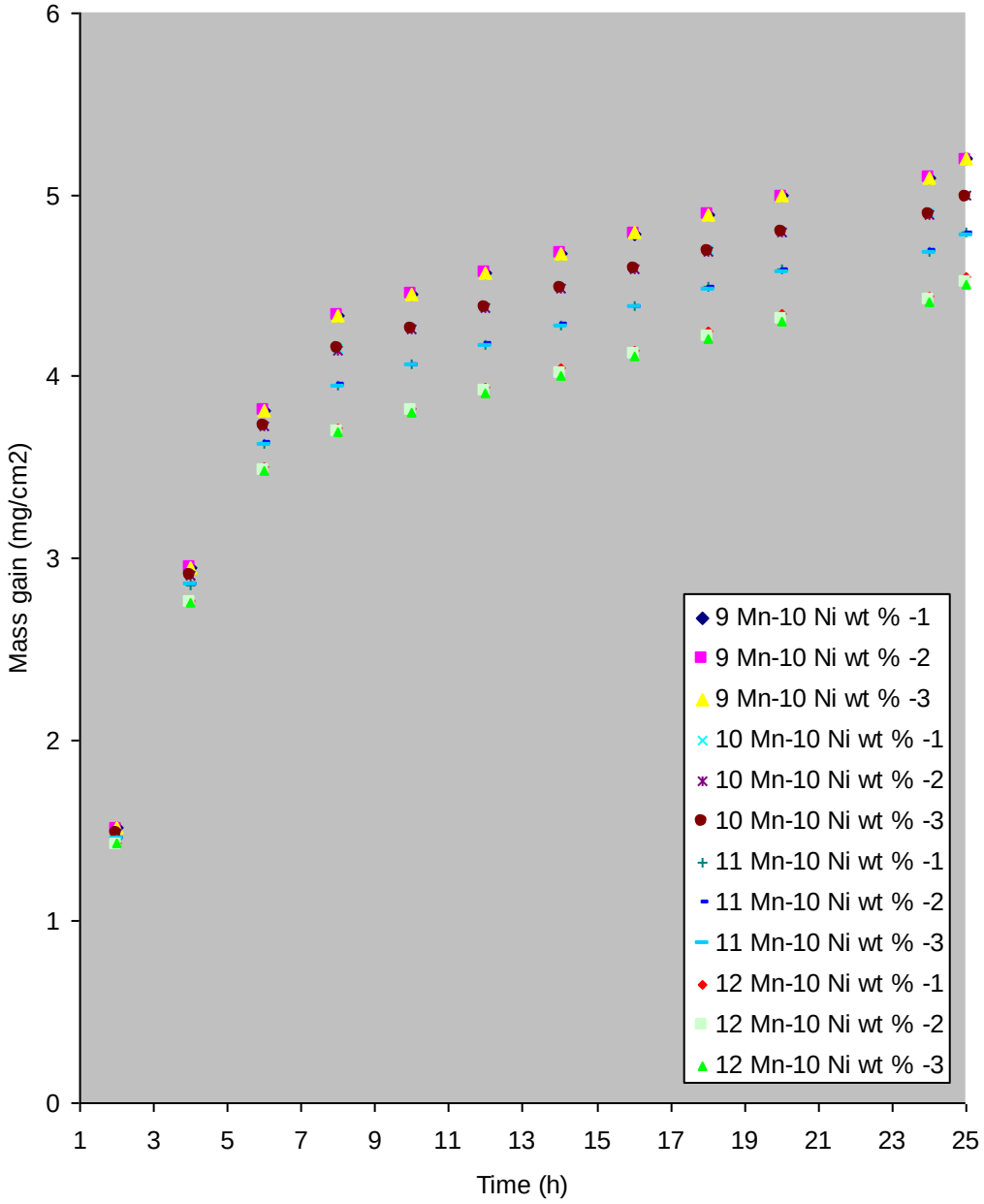

Fig. 4. The alloyed iron corroded for 25 hours at 765°C in furnace atmosphere-air

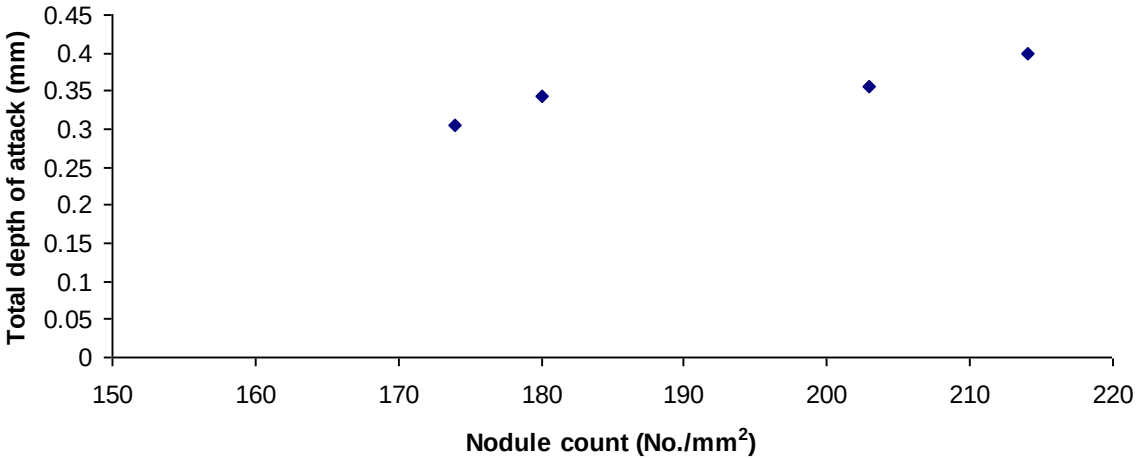

Fig. 5. Nodule count and overall depth of the oxidation attack

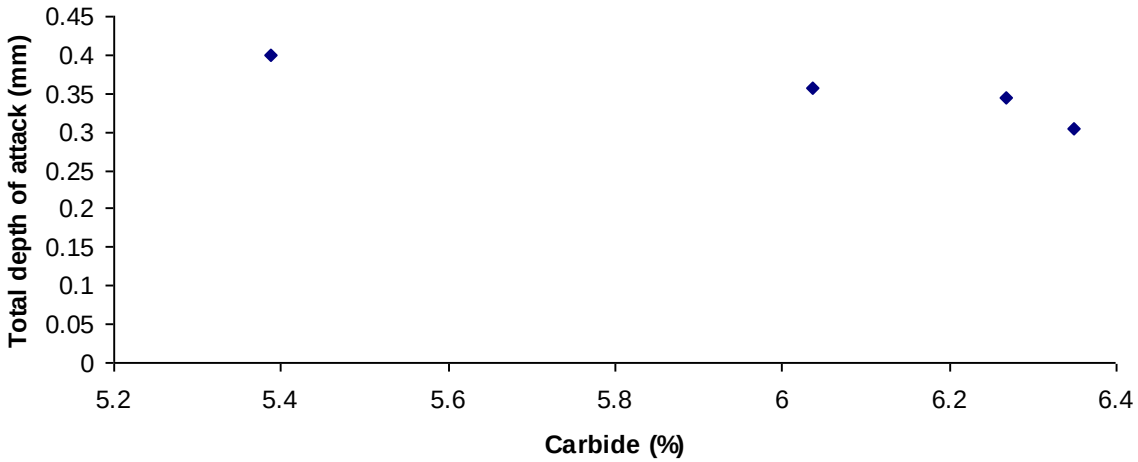

Fig. 6. % of carbide and overall depth of oxide assault

Figure 7 depicts the surface and cross section morphologies of alloyed iron that has been corroded for 25 hours at 765°C in a furnace environment with air. The oxide's black surface has whiskers all over it. After 25 hours, cooling caused the majority of the exterior Fe oxide layer to spall off. It was made up of tiny oxide precipitates that were mixed with a matrix of iron, manganese, and nickel. The lower Cr content employed during melting is the cause of the absence of Cr oxide. Awaruite, taenite, nickel iron oxide, $MnFe_2O_4$, and $NiFe_2O_4$ were the Fe oxides that made up the outer oxide layer. Large slabs of this outer oxide spalled off violently [13]. Due to the stress brought on by the formation of oxide during the oxidation period, oxide spallation occurred. As the weight continued to increase, the stress and oxide growth began to build up. The scale thickness could no longer support the mounting pressure at a particular point and released it. Oxide began to crack and spall due to this discharge [14,15]. SiO_2, wustite, hematite, magnetite, iron manganese oxide, and austenite structure made up the inner oxide. Higher Mn/wt% was less corroded and had a lower oxide thickness, according to both inner oxide thickness measurements. Additionally, SiO_2, which is well-known for its abilities to prevent oxidation, is present [16].

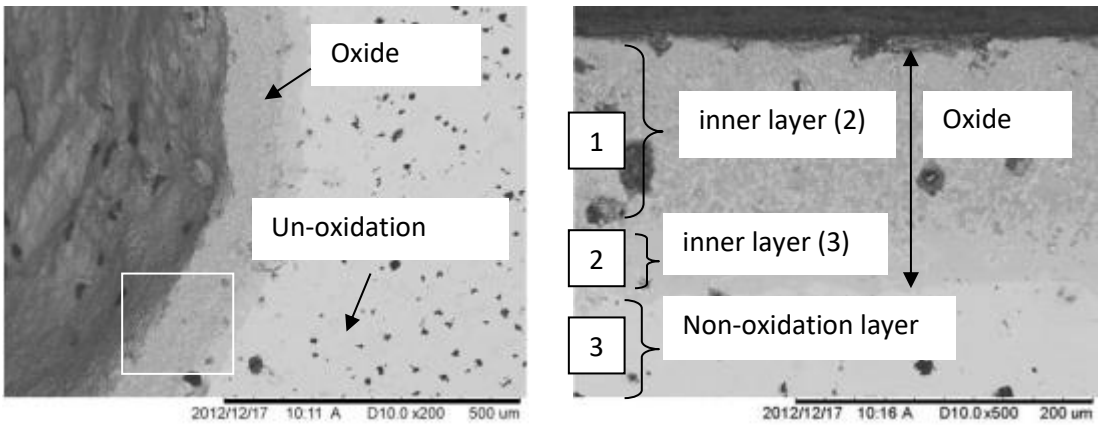

(a) (b)

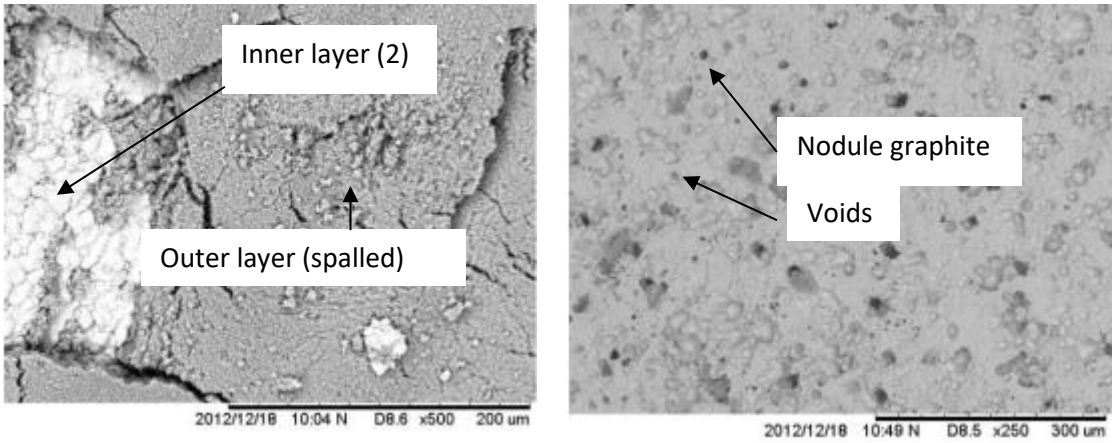

(c) (d)

Fig. 7. SEM micrograph of alloyed iron that had been corroding in furnace atmosphere-air for 25 hours at 765°C

4. Conclusions

In this study, an alloyed iron (manganese, iron, and nickel oxide) generated a mixture of exterior oxide scale and inside oxide of some elements. Awaruite, Taenite, $MnFe_2O_4$, and NiFe2O4 made up the outer layer, whereas SiO_2, Wustite, Hematite, Magnetite, $MnFe_2O_4$, and Austenite made up the interior layer. These layers developed as a result of internal iron oxides precipitating and penetrating the exterior scale in the alloy. Precipitation is most likely caused by the action of specific components, like the inward diffusion of oxygen. Because changed phases occur at high temperatures, more manganese addition does degrade tensile characteristics. In the microstructure, free nodular graphite predominates over carbide formation. Thus, the crack arrester characteristic responsible for the nodule graphite becomes less.

Acknowledgement

This research was funded by a grant from Ministry of Higher Education of Malaysia (FRGS Grant FRGS/1/2022/TK10/UMP/02/64 - RDU220135) and university's internal grant (RDU220305).

References

[1] Çelik, Gülşah Aktaş, Maria-Ioanna T. Tzini, Şeyda Polat, Ş. Hakan Atapek, and Gregory N. Haidemenopoulos. "Thermal and microstructural characterization of a novel ductile cast iron modified by aluminum addition." *International Journal of Minerals, Metallurgy and Materials* 27 (2020): 190-199. https://doi.org/10.1007/s12613-019-1876-8

[2] Xiang, Shengmei, Stefan Jonsson, Baohua Zhu, and Joakim Odqvist. "Corrosion fatigue of austenitic cast iron Ni-Resist D5S and austenitic cast steel HK30 in argon and synthetic diesel exhaust at 800° C." *International Journal of Fatigue* 132 (2020): 105396. https://doi.org/10.1016/j.ijfatigue.2019.105396

[3] Fatahalla, Nabil, Aly AbuElEzz, and Moenes Semeida. "C, Si and Ni as alloying elements to vary carbon equivalent of austenitic ductile cast iron: Microstructure and mechanical properties." *Materials Science and Engineering: A* 504, no. 1-2 (2009): 81-89. https://doi.org/10.1016/j.msea.2008.10.019

[4] Morrison, J. C. "Corrosion behaviour of Ni-Resist cast irons." *Anti-Corrosion Methods and Materials* 30, no. 8 (1983): 8-9. https://doi.org/10.1108/eb007227

[5] Jincheng, Xu. "Ecodesign for wear resistant ductile cast iron with medium manganese content." *Materials & Design* 24, no. 1 (2003): 63-68. https://doi.org/10.1016/S0261-3069(02)00076-6

[6] Choi, J. O., J. Y. Kim, C. O. Choi, J. K. Kim, and P. K. Rohatgi. "Effect of rare earth element on microstructure formation and mechanical properties of thin wall ductile iron castings." *Materials Science and Engineering: A* 383, no. 2 (2004): 323-333. https://doi.org/10.1016/j.msea.2004.04.060

[7] Jiyang, Zhou. "Colour metallography of cast iron." *China Foundry* 6, no. 2 (2009): 152-163. https://doaj.org/article/57b0e76ccada47119c9ba8bee4406452
[8] Dias, Anderson, and Vanessa de Freitas Cunha Lins. "Scale morphologies and compositions of an iron-manganese-aluminum-silicon alloy oxidated at high temperatures." *Corrosion Science* 40, no. 2-3 (1998): 271-280. https://doi.org/10.1016/S0010-938X(97)00134-0
[9] Tjong, S. C. "Electron microscope observations of phase decompositions in an austenitic Fe-8.7 Al-29.7 Mn-1.04 C alloy." *Materials Characterization* 24, no. 3 (1990): 275-292. https://doi.org/10.1016/1044-5803(90)90055-O
[10] Rashidi, Maarof Mohd, and Mohd Hasbullah Idris. "Microstructure and mechanical properties of modified ductile Ni-resist with higher manganese content." *Materials Science and Engineering: A* 574 (2013): 226-234. https://doi.org/10.1016/j.msea.2013.02.038
[11] Kim, Yoon-Jun, Ho Jang, and Yong-Jun Oh. "High-temperature low-cycle fatigue property of heat-resistant ductile-cast irons." *Metallurgical and Materials Transactions A* 40 (2009): 2087-2097. https://doi.org/10.1007/s11661-009-9911-4
[12] Velasco, F., A. Bautista, and A. González-Centeno. "High-temperature oxidation and aqueous corrosion performance of ferritic, vacuum-sintered stainless steels prealloyed with Si." *Corrosion Science* 51, no. 1 (2009): 21-27. https://doi.org/10.1016/j.corsci.2008.09.035
[13] Cao, G., V. Firouzdor, K. Sridharan, M. Anderson, and T. R. Allen. "Corrosion of austenitic alloys in high temperature supercritical carbon dioxide." *Corrosion Science* 60 (2012): 246-255. https://doi.org/10.1016/j.corsci.2012.03.029
[14] Heo, Jun, Jaewoo Lee, Sungwoo Kim, Akram Alfantazi, and Sung Oh Cho. "Corrosion resistance of austenitic stainless steel using cathodic plasma electrolytic oxidation." *Surface and Coatings Technology* 462 (2023): 129448. https://doi.org/10.1016/j.surfcoat.2023.129448
[15] Cai, Yuchen, Thuan Dinh Nguyen, Jianqiang Zhang, Brian Gleeson, and David J. Young. "Corrosion behaviour of Fe-based austenitic and Ni-based alloys in Wet CO_2 gas with and without chloride deposits at 650° C." *Corrosion Science* 210 (2023): 110822. https://doi.org/10.1016/j.corsci.2022.110822
[16] Chen, K., J. Wang, L. Zhang, H. Wang, X. An, Y. Li, J. Zhang, Z. Shen, and X. Zeng. "A high-resolution study of the different surface state effects on the corrosion behaviors of a ferritic steel and an austenitic steel in supercritical water." *Corrosion Science* 209 (2022): 110757. https://doi.org/10.1016/j.corsci.2022.110757